



Hexagonal Co₆ and Zigzag Co₄ Clusters Based Magnetic MOFs with pcu Net for Selective Catalysis

Journal:	<i>Inorganic Chemistry Frontiers</i>
Manuscript ID	QI-RES-08-2015-000159.R1
Article Type:	Research article
Date Submitted by the Author:	06-Oct-2015
Complete List of Authors:	Yao, Ru-Xin; Shanxi Normal University, Qiao, Xiao-Hui; Shanxi Normal University, School of Chemistry and Material Science Cui, Xin; Shanxi Normal University, School of Chemistry and Material Science Jia, Xiao-Xia; Shanxi Normal University, School of Chemistry and Material Science Zhang, Xian-Ming; Shanxi Normal University, School of Chemistry and Material Science



Journal Name

ARTICLE

Hexagonal Co₆ and Zigzag Co₄ Clusters Based Magnetic MOFs with *pcu* Net for Selective Catalysis

Ru-Xin Yao, Xiao-Hui Qiao, Xin Cui, Xiao-Xia Jia, and Xian-Ming Zhang*

Received 00th January 20xx,
Accepted 00th January 20xx

DOI: 10.1039/x0xx00000x

www.rsc.org/

Two hydrophobic 3D cobalt-cluster based magnetic MOFs, [Co₃(pimdc)₂(H₂O)₆]·5H₂O (**1**) and Co₂(Hpimdc)₂ (H₃pimdc = 2-propyl-imidazole-4,5-dicarboxylic acid) have been hydrothermally synthesized and magnetically characterized. Both of them exhibit regular *pcu* net with hexagonal Co₆ and zigzag Co₄ clusters as 6-connected nodes, respectively. The magnetic studies indicate that **1** displays predominant antiferromagnetic interactions within Co₃(pimdc) triangle, while **2** shows spin-canting antiferromagnetic behaviour with larger canting angles. Furthermore, after heating in vacuum condition, activated **1** exhibits an excellent catalytic selectivity in the allylic oxidation reaction of cyclohexene to formation of α , β -unsaturated ketone, which indicates that the opened Co(II) sites play a significant role in heterogeneous catalytic process.

1. Introduction

Metal-organic frameworks (MOFs) have attracted considerable attention for charming topologies and potential applications in molecular magnetism, chemical sensor, heterogeneous catalysis and drug delivery.¹⁻³ Modular chemistry has become an effective strategy to construct multifunctional magnetic materials,⁴ due to transition metal clusters as secondary building blocks (SBUs) could not only efficiently reduce the coordination number and geometric limitation, but also modulate the properties of MOFs as functional carriers. Hexagonal ring and zigzag clusters are relatively scarce in various cobalt clusters bridged vertex-sharing or edge-sharing. Only several complexes with hexagonal M₆ cluster have been documented, such as discrete Pd₆ molecular,⁵ homochiral Fe₆ wheels,⁶ a binodal (3,18) connected 3D net⁷ constructed by cyclo-cluster [Co₆(COO)₆(H₂O)₁₂]⁶⁺ and two Co₆ cluster based 3D polymers with 2-position aromatic substituent of imdc³⁻ ligand.⁸

On the other hand, the oxidation of cyclic olefin, especially selective formation of α , β -unsaturated ketones, is important in chemical industry as well as value-added fine chemicals.⁹ However, heterogeneous transition-metal catalysts are still limited and most reports about the oxidation of cyclohexene by MOFs catalysts mainly produce tert-butyl-2-cyclohexenyl-1-peroxide.¹⁰ MOFs provide a great platform to develop heterogeneous catalysis, due to their high catalyst loadings

and more accessible and identifiable catalytic centers. However, it is still facing great challenge to assemble metal cluster-based multifunctional magnetic materials, especially selective catalyst for the oxidation of cyclohexene.

In our previous research on coordinated diversity of cadmium 4,5-imidazoledicarboxylate (H₃imdc) framework,¹¹ we found that H₃imdc is a rigid ligand with versatile coordination modes and acidity-dependent property, which has been successfully assembled high dimension structures and zeolite frameworks due to the M-im-M angle is similar to the average Si-O-Si angle (145°).¹² Recently, this system has been extended by simple modification of the 2-position imidazole ring with alkyl (Me, Et, Pr) and aromatic phenyl, which may generate significant effect on the final structure, but search of the CSD database reveals that only several low dimension polymers were reported, such as square tetranuclear complexes, one-dimensional chain and two-dimensional layer.¹³ Using methyl or ethyl substituent imidazole ligand, Chen's group synthesized MAF-6 with exceptional hydrophobicity, which readily adsorb organic molecules; MAF-X8 thin films which can solid-phase micro-extract non-polar volatile organic compounds from polar phenols.¹⁴ Inspired by that work, herein we adopt 2-propyl imidazole-4,5-dicarboxylic acid (H₃pimdc) and present two hydrophobic 3D cobalt cluster based magnetic MOFs with regular *pcu* net, namely, Co₃(pimdc)₂(H₂O)₆]·5H₂O (**1**) and Co₂(Hpimdc)₂ (**2**), constructed by hexagonal Co₆ and zigzag Co₄ clusters, respectively. Magnetic studies indicated that **1** shows antiferromagnetic interactions within Co₃(pimdc) triangle, while **2** displays spin-canting antiferromagnetic behavior with larger canting angles. Furthermore, after heating in vacuum condition, activated **1** exhibits an excellent catalytic selectivity in the allylic oxidation reaction of cyclohexene to formation of

^a School of Chemistry & Material Science, Shanxi Normal University, Linfen 041004, P. R. China.

* E-mail: zhangxm@dns.sxnu.edu.cn.

Electronic Supplementary Information (ESI) available: CCDC 1409462-1409463 See DOI: 10.1039/x0xx00000x

α , β -unsaturated ketone with tert-butyl hydroperoxide (*t*-BuOOH) as oxidant.

2. Experimental section

2.1 Materials and physical measurements

All chemicals were analytically pure from commercial sources and used without further purification, unless otherwise noted. 1, 2, 4-trichlorobenzene was chromatographically pure. Cyclohexane and cyclohexene were dried by anhydrous CaCl₂. *t*-BuOOH was dried by anhydrous MgSO₄ in an ice bath. Elemental analyses were performed on a Vario EL-II analyzer. FTIR spectra were recorded from KBr pellets in the range 4000–400 cm⁻¹ on a Nicolet 5DX spectrometer. Powder X-ray diffraction (PXRD) data were collected in a Bruker D8 advance diffractometer (Cu_{K α} , λ = 1.5418 Å). The thermo-gravimetric analysis (TG) was carried out under air atmosphere using SETARAM LABSYS equipment at a heating rate of 10 °C/min. The magnetic measurements were made with Quantum Design SQUID MPMS XL-5 instruments. The magnetic data were corrected for the diamagnetism of the samples using Pascal constants. N₂ adsorption measurement was performed using a Micromeritics ASAP 2020HD88 surface area and pore size analyzer, which was conducted up to a relative pressure (p/p_0) of 1.0 at STP.

2.2 Synthesis of [Co₃(pimdc)₂(H₂O)₆]·5H₂O (**1**)

A mixture of Co(NO₃)₂·6H₂O (0.030 g, 0.10 mmol), H₃pimdc (0.029 g, 0.20 mmol), [N(CH₃)₄]Cl (0.012g, 0.1mmol) and H₂O (6 mL) was stirred, then sealed in a 15-mL teflon-lined stainless autoclave at 160 °C for 5 days. After it was cooled to room temperature and subjected to filtration, red block crystals of **1** in yield of 35.8% (based on pimdc) were recovered. Anal. calcd (%) for C₁₆H₂₉Co₃N₄O₁₇ (**1**): C, 26.46; H, 4.02; N, 7.71. Found: C, 26.51; H, 3.97; N, 7.68. IR data (KBr, cm⁻¹, Fig. S1): 3433(b), 2964(s), 1656(s), 1426(s), 1324(s), 1121(m), 1054(w), 875(w), 826(w), 767(w), 542(w).

2.3 Synthesis of Co₂(Hpimdc)₂ (**2**)

A mixture of Co(NO₃)₂·6H₂O (0.031 g, 0.15 mmol), H₃pimdc (0.041 g, 0.20 mmol), CH₃OH (1 mL) and H₂O (5 mL) was stirred, adjusted to pH = 6 by the addition of NaOH (0.008 g, 0.20 mmol), then sealed in a 15-mL teflon-lined stainless autoclave at 160 °C for 5 days. After it was cooled to room temperature and subjected to filtration, red cubic crystals of **2** in yield of 67.5% (based on pimdc) were recovered. Anal. calcd (%) for C₁₆H₁₄Co₂N₄O₈ (**2**): C, 37.82; H, 2.78; N, 11.03. Found: C, 37.78; H, 2.81; N, 11.01. IR data (KBr, cm⁻¹, Fig. S1): 3427(b), 2957(s), 2928(w), 2869(w), 1606(s), 1446(s), 1243(m), 1115(m), 1042(w), 869(w), 781(w), 544(w).

2.4 Crystallography studies

Single-crystal X-ray diffraction measurements were carried out at room temperature on an Agilent Gemini Eos diffractometer with graphite-monochromated Mo-K α radiation (λ = 0.71073

Å). The CrysAlisPro (Agilent Technologies) was used for absorption correction.¹⁵ All the structures were solved by direct methods and refined by full-matrix least-squares analysis with SHELXL-97 software.¹⁶ All non-hydrogen atoms were refined with anisotropic thermal parameters. Hydrogen atoms of organic ligand were generated theoretically onto the specific carbon and refined isotropically with fixed thermal factors. Further details for structural analysis are summarized in Table 1, corresponding bond lengths and bond angles are shown in Table S3.

Table 1. Crystallographic data and structure refinement of **1** and **2**

compound	1	2
Empirical	C ₁₆ H ₂₉ Co ₃ N ₄ O ₁₇	C ₁₆ H ₁₄ Co ₂ N ₄ O ₈
Fw	726.47	508.17
Crystal system	trigonal	Orthorhombic
Space group	<i>R</i> -3 <i>c</i>	<i>Pbam</i>
a (Å)	24.4314(6)	15.9765(17)
b (Å)	24.4314(6)	15.0880(15)
c (Å)	27.9400(9)	15.9616(16)
α (°)	90	90
β (°)	90	90
γ (°)	120	90
V (Å ³)	14442.9(9)	3847.6(7)
Z	18	8
ρ_{calc} (g cm ⁻³)	1.503	1.755
μ (mm ⁻¹)	1.603	1.778
<i>F</i> (000)	6664	2048
Crystalsize (mm)	0.20×0.16×0.10	0.22×0.16×0.12
Reflections	11498 / 3288	22442 / 4089
<i>T</i> _{max} / <i>T</i> _{min}	0.994 / 1.000	0.703 / 1.000
Data / parameters	3288 / 213	4089 / 312
<i>S</i>	1.046	1.048
<i>R</i> ₁ ^a , <i>wR</i> ₂ ^b [<i>I</i> > 2 σ (<i>I</i>)]	0.0319, 0.0912	0.0568, 0.1641
<i>R</i> ₁ , <i>wR</i> ₂ (all data)	0.0398, 0.0948	0.0715, 0.1769
$\Delta\rho_{\text{max}} / \Delta\rho_{\text{min}}$ (eÅ ⁻³)	0.61 / -0.36	1.22 / -0.96

$$^a R_1 = \sum ||F_o| - |F_c|| / \sum |F_o|, \text{ b. } wR_2 = [\sum w(F_o^2 - F_c^2)^2 / \sum w(F_o^2)^2]^{1/2}$$

2.5 Catalytic oxidation of cyclohexene

Compound **1** was immersed in methanol for 3 days to remove the guest water molecules, and fresh methanol was changed at least three times a day after the extract was decanted. Then the sample was dried under a vacuum at 100 °C overnight to obtain activated **1**, during which crystal color changed from red to purple (Fig. S2). Activated **1** was added to a solution of cyclohexene (3.8 mmol), *t*-BuOOH (14 mmol) and 1, 2, 4-trichlorobenzene (1 mmol, as internal standard). The reaction mixture was stirred at 70 °C. Aliquots of reaction mixture (0.1 mL) were removed after time interval, and diluted with cyclohexane (1 mL) and filtered through a 0.25 mm Acrodisc

nylon filter. Then, the sample was identified by GC-MS and quantified by GC. For investigations on catalyst activity, the catalyst was separated from the reaction mixture by centrifugation and rinsed five times with cyclohexane before reused. The reaction progress was monitored by GC analysis, which performed using Agilent 7820 GC with a cross-linked (95%)-dimethyl-(5%)-diphenylpolysiloxane (HP-5, 30 m \times 0.32 mm \times 0.25 μ m), injector temperature 280 $^{\circ}$ C, FID detector temperature 300 $^{\circ}$ C, and oven temperature program 40 $^{\circ}$ C (3 min) -20 $^{\circ}$ C/min - 250 $^{\circ}$ C (2 min). GC/MS analysis was performed using a Thermo Fisher Polaris Q (Ion Trap) gas chromatograph / mass spectrometer.

3. Results and discussion

3.1 Description of Structure

Single-crystal X-ray diffraction analysis reveals that compound **1** crystallizes in the trigonal space group $R\bar{3}c$, and the asymmetric unit consists of two crystallographic independent Co^{2+} ions, one pimdc^{3-} ligand, three terminal coordinated water molecules, two and a half crystal lattice water molecules (Fig. 1a). All of the atoms, except for C7, C8 and Co2, localize in general positions. Both Co centers adopt octahedral coordination environments with $[\text{CoN}_2\text{O}_4]$ and $[\text{CoO}_6]$ modes, respectively. The Co1 is coordinated by two nitrogen atoms from two imidazole groups, two carboxylate oxygen atoms and two terminal water molecules. Comparatively, the Co2 is located at the center of inversion with site occupancy of 0.5, which equatorial plane occupied by four carboxylate oxygen atoms from two different pimdc^{3-} ligands, and the axial positions occupied by two terminal water molecules. Additionally, the carbon atoms of propyl group (C7, C8) are disordered, located on the c -position glide plane. The Co-L (L = N or O) bond lengths are in the range of 2.038(2)-2.182(3) \AA . The *cis* and *trans* L-Co-L (L = N or O) bond angles are within the range 78.32(9)-106.77(9) $^{\circ}$ and 159.47(10)-180.00(13) $^{\circ}$, respectively. Based on the unique equicrural triangle bridging mode of the pimdc^{3-} ligand *i.e.* $\mu_3\text{-KN,O} : \text{kO}',\text{O}'' : \text{kN}',\text{O}'''$ (Fig. S3), six Co(1) atoms form a regular hexagonal ring $[\text{Co}_6(\text{pimdc})_6]$ with neighboring $\text{Co}^{\text{III}}\text{Co}$ distance is 6.2715(9) \AA . Meanwhile, Co(2) atoms alternately point up and down the hexagonal plane, looking like a royal crown $[\text{Co}(1)_6\text{Co}(2)_6(\text{pimdc})_6]$ (Fig. 1b). Moreover, countless hexagonal rings constitute the honeycomb-like 3D framework with a distinct hydrophobic void, which is filled by flexible propyl groups (Fig. 1c). Calculation with *PLATON* reveals that free volume of per unit cell is 1828.8 \AA^3 (12.7% of the total volume). Solvent contact angle measurement is carried out to assess the particle surface property of **1**. Interestingly, a water droplet can maintain its shape and powder of **1** can float on the water surface (Fig. S4a). But powder of **1** exhibit a wet crystal surface with a smaller contact angle for ethanol and can't float on the ethanol surface (Fig. S4b), which confirms that the higher affinity for polar solvent and the hydrophobic nature of the pore surface of **1**. From a topological point of view, the hexagonal ring $[\text{Co}_6(\text{pimdc})_6]$ can be considered as a 6-

connected node which links with six neighboring $[\text{Co}_6(\text{pimdc})_6]$ units *via* Co(2) linkers (Fig. S5a). Based on this simplification, the overall 3D framework of **1** can be described as an uninodal 6-connected *pcu* topology with the short *Schläfli* symbol of $(4^{12}\cdot 6^3)$. To the best of our knowledge, *pcu* topology is one of the five regular prototypical nets, and diversified vertex-sharing / edge-sharing hexanuclear cobalt clusters have been reported as 6-connected nodes,^{17,18} but few of *pcu* frameworks with hexagonal Co_6 clusters.

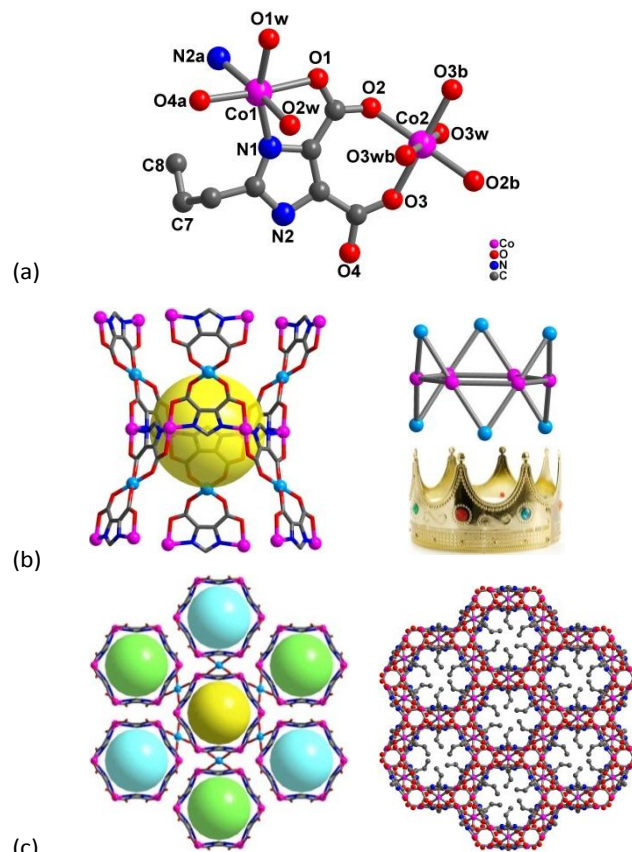


Fig. 1 (a) Coordination environment of the Co^{2+} ions, (b) the hexagonal Co_6 unit looks a royal crown, (c) Co_6 cluster is linked by six clusters along a -axis direction and the honeycomb-like 3D framework with *pcu* topology in **1** (note : propyl group is deleted for clarity in plot (b)).

Compound **2** crystallizes in the orthorhombic space group $Pbam$, and the asymmetric unit consists of two crystallographic independent Co^{2+} ions and three Hpimdc^{2-} ligands, of which two ligands are mirror symmetric along propyl group (Fig. 2a). The propyl group is also disordered, and carbon atoms of propyl group (C12, C13, C14, C18, C19, C20), C9 and C15 locate on the mirror plane with site occupancy of 0.5. Both Co^{2+} centers adopt octahedral geometry with $[\text{CoN}_2\text{O}_4]$ mode, and they are coordinated by two nitrogen atoms from two imidazole groups and four carboxylate oxygen atoms from four different Hpimdc^{2-} ligands. The Co-O distances are in the range of 2.101(3)-2.222(4) \AA and Co-N length are 2.051(3)-2.092(3) \AA . The *cis* and *trans* L-Co-L (L = N or O) angles are within the range 75.75(11)-119.49(13) $^{\circ}$ and 149.17(13)-173.18(13) $^{\circ}$, respectively. The pimdc^{2-} ligand adopts $\mu_4\text{-KN,O} : \text{kO}' : \text{kO}'' : \text{kN}',\text{O}''$ and $\mu_4\text{-KN,O} : \text{kO} : \text{kO}' :$

kN',O' modes bridging Co(1) and Co(2) ions (Fig. S3). To be noted, edge-sharing Co(2) dimer is linked with one Co(1) atom through edge-sharing mode by carboxylate oxygen atoms (O5 and O8), thus form a zigzag Co_4 cluster with $Co\cdots Co$ distance of 3.33–3.35 Å, and the angle of Co1–Co2–Co2a is 107.949(18)° (Fig. 2b). The Co_4 cluster is centrosymmetric with the inversion center located at the midpoint of two Co(2) ions, and only several complexes with zigzag Co_4O_6 core, may be due to it is apt to form an infinite cobalt chain.¹⁹ Each Co_4 SBUs is surrounded by four Hpimdc²⁻ ligands, meanwhile, each Hpimdc²⁻ ligand is connected by two tetramer to yield a 2D (4,4) rhombic grid (Fig. 2c and Fig. S5b). Adjacent layers are further linked by $\mu_4-kN,O : kO : kO' : kN',O'$ modes of Hpimdc²⁻ ligands to form a 3D framework (Fig. 2d). It is also an uninodal 6-connected pcu topology with a short Schläfli symbol of $(4^{12}\cdot 6^3)$, in which the zigzag Co_4 clusters are regarded as 6-connected nodes and Hpimdc²⁻ ligands as linkers.

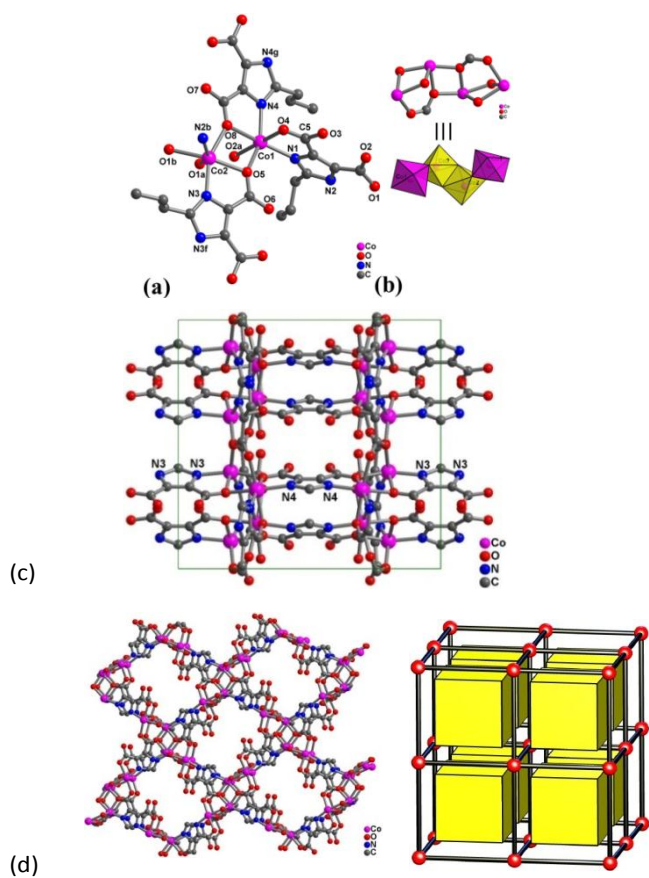


Fig. 2 (a) Coordination environment of Co^{2+} atoms, (b) the tetranuclear Co_4O_6 unit, (c) 2D rhombic grid along a -axis direction, (d) 3D framework with an uninodal 6-connected pcu topology in **2** (note : propyl group is deleted for clarity).

3.2 Thermal properties and PXRD

TG/DTA analyses of **1** and **2** were performed to examine thermal stabilities on polycrystalline samples in air atmosphere at the heating rate of 10 °C min⁻¹. Compounds **1-2** have same pcu networks but different coordinated environment, which results in different thermal stabilities (Fig. S6). For **1**, the initial weight loss of about 24.41% (*calcd* 26.06%) in the temperature

range of 20–130 °C corresponds to the removal of free and coordinated water molecules. The framework is stable up to around 300 °C in air atmosphere. The second weight loss in the temperature range of 300–600 °C is in agreement with the removal of pimdc²⁻ groups, accompanied by the decomposition of the framework. The final residues of 30.70% (*calcd* 31.71%) for **1** are close to the percentage of Co_3O_4 . On the contrary, the TG curve shows that **2** is stable up to 350 °C (Fig. S6), which may be ascribed to without terminal coordinated water molecules of Co^{2+} in **2**. The DTA plot of **1** present one endothermic peak at 130 °C and two exothermic peaks *ca.* 360 °C, while that of **2** exhibits two endothermic peaks at 393 and 478 °C. The phase purity of the bulk samples **1** and **2** are confirmed by the PXRD. Most peak positions of simulated and experimental patterns are in good agreement with each other. The dissimilarities in intensity may be due to the preferred orientation of the crystalline powder samples (Fig. S7).

3.3 Magnetic Studies

Magnetic susceptibility was measured on phase-pure samples of **1-2** in the temperature range 300–2 K at a field of 1000 Oe. For **1**, the $\chi_m T$ value per Co_3 unit is 8.26 cm³ K mol⁻¹ at room temperature, which is much higher than the expected value of 5.625 cm³ K mol⁻¹ for three magnetically isolated high-spin Co^{2+} ions with $S = 3/2$ and $g = 2.00$, owing to the significant orbital contribution of Co^{2+} ions in an octahedral environment.²⁰ Upon cooling, the $\chi_m T$ value gradually decreases to reach a minimum of 0.82 cm³ K mol⁻¹ at 2 K. Such decrease is a characteristic of dominant antiferromagnetic (AF) exchange interactions as well as the effect of spin-orbit coupling in Co^{2+} ions. Between 300 and 10.0 K, the susceptibility obeys the Curie-Weiss law with a Curie constant of $C = 9.006(3)$ cm³ K mol⁻¹ and Weiss constant $\theta = -28.383(4)$ K (Fig. 3a). The C value gives rise to an average g value of 2.53,

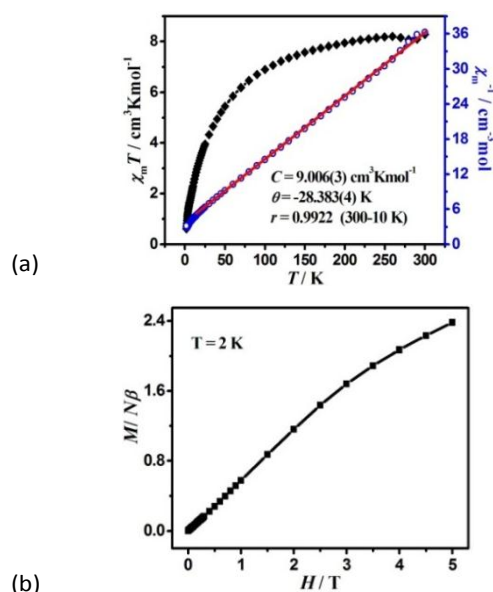


Fig. 3 (a) The $\chi_m T$ versus T plots and the Curie-Weiss fitting of χ_m^{-1} versus T curves for **1** under an applied dc 1000 Oe field per Co_3 unit, (b) field dependence of magnetization at 2 K.

being normal for an octahedral Co^{2+} ion. The large negative value of the Weiss constant indicates AF interaction between Co^{2+} ions. The magnetization of **1** at 2 K increases slowly and linearly with the applied field. The field-dependent magnetization at the highest field 5 T is $2.38 N\beta$ (Fig. 3b), far below the saturation value of $9 N\beta$ expected for three spin-only Co^{2+} ions, but close to the value of one spin-only Co^{2+} ion, revealing the presence of antiferromagnetic interactions in the material which may be associated with spin frustrated Co_3 triangles.²¹ Nevertheless, we cannot establish an appropriate magnetic model to determine the magnetic coupling constant of metal ions, due to **1** is a complicated metal crown type 3 D framework.

For **2**, the $\chi_m T$ value per Co_4 unit is $11.69 \text{ cm}^3 \text{ K mol}^{-1}$ at room temperature, which is much higher than the expected value of $7.5 \text{ cm}^3 \text{ K mol}^{-1}$ for four magnetically isolated high-spin Co^{2+} ions with $S = 3/2$ and $g = 2.00$, owing to the significant orbital contribution of Co^{2+} ions in an octahedral environment. The $\chi_m T$ value at room temperature corresponds to effective magnetic moments $4.84 \mu_B$ per Co, which is in accordance with the documented orbital contribution of high-spin Co^{2+} ion. As the temperature decreasing, the $\chi_m T$ value first decreases smoothly to a minimum of $2.08 \text{ cm}^3 \text{ K mol}^{-1}$ at about 6.29 K, which is caused by spin-orbit coupling or antiferromagnetic interactions. Upon further lowering the temperature, the $\chi_m T$ rises abruptly to a maximum value of $7.13 \text{ cm}^3 \text{ K mol}^{-1}$ at 3.49 K, and finally drops to $4.31 \text{ cm}^3 \text{ K mol}^{-1}$ at 2 K (Fig. 4a). This is a character of the spin-canted antiferromagnetic behaviour, and further confirmed by the field dependence of magnetic susceptibility at 2K, being larger at a smaller field (Fig. S8). Between the temperature range of 300 to 9.0 K, the inverse molar susceptibility vs T plot is linear and obeys the Curie-Weiss law with the Curie constant $C = 13.03(4) \text{ cm}^3 \text{ K mol}^{-1}$ and Weiss constant $\theta = -38.67(5) \text{ K}$. The C value gives rise to an average g value of 2.64, being normal for an octahedral Co^{2+} ion. The negative Weiss constant θ of **2** indicates AF interaction between Co^{2+} ions.

The M vs H curve at 2 K displays the magnetization increase rapidly to $0.34 N\beta$ at low field 365 Oe and further reaches linearly to $2.28 N\beta$ per Co_4 unit at 5T (Fig. 4b), far below the saturation value of $12 N\beta$ for four spin-only Co(II) ions, suggesting a canted antiferromagnet behaviour. Field-cooled (FC) and zero-field-cooled (ZFC) magnetizations are performed under an applied field of 10 Oe, and the bifurcation at 5.27 K indicates the occurrence of long-range magnetic ordering below this temperature (Fig. 4c). A narrow hysteresis loop is observed at 2 K with the remnant magnetization M_R of $0.524 N\beta$ and the coercive field of 204 Oe for **2** (Fig. 4d). Canting angle can be roughly estimated through the equation $\sin(\gamma) = M_R/M_S$ to be 3.49° , assuming $M_S = 8.60 N\beta$ for four octahedral Co^{2+} ions (at low temperature, the effect spin $S = 1/2$ with an average g of 4.3 for octahedral Co^{2+} ions). It should be pointed out that weak ferromagnets with large canting angles are relatively rare.²² Generally, spin-canting arises due to two factors: (i) the single-ion magnetic anisotropy and (ii) anti-symmetric exchange interaction, namely Dzyaloshinskii-Moriya interaction (DMI). The study of the structure of **2**

reveals that the large canting angle originate from the anti-symmetric exchange in the zigzag Co_4 cluster.

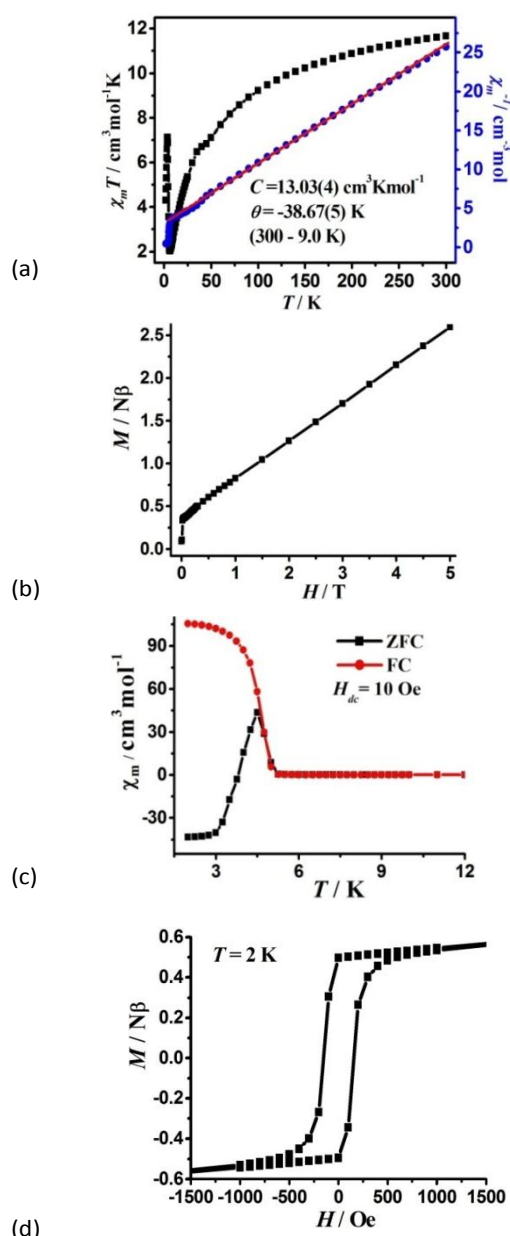


Fig. 4 (a) The $\chi_m T$ versus T plots and the Curie-Weiss fitting of χ_m^{-1} versus T curves under an applied d_c 1000 Oe field per Co_4 unit, (b) field dependence of magnetization at 2 K, (c) FC and ZFC magnetization at 10 Oe, and (d) the hysteresis loop at 2 K for **2**.

Neglecting single-ion anisotropy or spin-orbit coupling of metal ions, simulation of the temperature dependence of $\chi_m T$ values for **2** has been attempted with the Heisenberg Hamiltonian equation (1):

$$\hat{H}_{ex} = -2J_1(S_1S_2 + S_3S_4) - 2J_2S_2S_3 \quad (1)$$

Two exchange coupling constants were adopted for the zigzag Co_4 cluster based complex **2**: J_1 stands for exchange interaction of $\text{Co}(1)\cdots\text{Co}(2)$ ions, while J_2 stands for that of two $\text{Co}2$ ions with $S_1 = S_2 = S_3 = 3/2$. The best parameters fitted in the range 10–300 K are $J_1 = -4.3 \text{ cm}^{-1}$, $J_2 = -13.5 \text{ cm}^{-1}$, and $g = 2.65$ for **2**

(Fig. 5). The negative J value indicates antiferromagnetic interactions between Co^{2+} ions within Co_4O_6 cluster, which can be understood based on structural feature. There are three magnetic delivered pathways between $\text{Co}^{\text{III}}\text{Co}$ ions: two $\mu_2\text{-O}$ bridges with the Co-O-Co angle of 103.32° , 102.52° and 100.82° , and one *syn-syn* carboxylate bridge. Generally, Co-O-Co angle greater than 100° and carboxylate *syn-syn* mode transfer AF interactions.²³ Therefore, it is reasonable to assume that intra-cluster Co_4 is AF coupling.

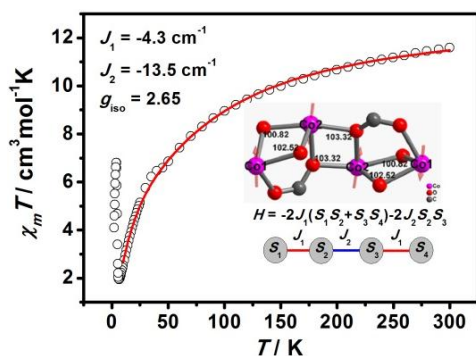


Fig. 5 The best fitting of experimental data using Heisenberg Hamiltonian model for **2**.

3.4 Allylic oxidations of cyclohexene with **1** as catalyst

For compound **1**, due to each Co(II) center has two terminal water molecules which could be lost and provide coordinative unsaturated metal center as Lewis acid catalytic sites. The oxidation reaction of cyclohexene with *t*-BuOOH oxidant was used as a catalytic test reaction. To select the optimal experimental conditions, the effects of particle size, amount of catalyst and temperature were investigated, respectively, when fixed other reaction conditions. In the presence of catalyst **1**, the conversion increased with the reaction temperature from 50 to 70 °C, but decreased beyond 70 °C (Table S1, entry 4-8), which may be due to the decomposition of *t*-BuOOH without oxidizing cyclohexene. The higher conversion achieved with a smaller amount of **1** (Table S1, entry 1-4). Thus, the optimal conditions is loading of 0.10 mmol activated **1** at 70 °C 20 hours under solvent-free conditions (shown in Fig. 6). The TON was as high as about 148 (Table S1, entry 6). Table S2 is the comparison of catalytic properties of activated **1** with some representative catalysts for the allylic oxidation of cyclohexene. Transition metal cobalt salts showed the highest conversion and α , β -unsaturated ketone selectivity,²⁴ but they are homogeneous catalysts, which is difficult for separation and recyclable use. Compound **1** is heterogeneous catalyst, which offers advantages over homogeneous catalysts, such as easy separation, efficient recycling, improved handling and process control. It is noted that heterogeneous catalysts $\text{Fe}^{\text{III}}/\text{SiO}_2$ and Co-MOF provide higher conversion but need organic solvent CH_3CN .^{25,26} However, **1** is a green catalyst, and shows conversion close to the highest catalyst Cr-MIL-101 to date.²⁷ Although **1** has a hydrophobic pore (12.7% of the total volume) calculated by PLATON, flexible propyl groups might hinder reactants enter into the pore, which is confirmed by the negligible N_2

adsorption at 77 K with a Langmuir surface area of $41.10 \text{ m}^2 \text{ g}^{-1}$ (Fig. S9), suggesting that the catalytic reaction is primarily occurred on the catalyst surface. As comparative experiment, **1** (without activated) and **2** were used as catalyst under the same condition, about 3.8 % or 3.3 % conversion were obtained after 20 hours, which is close to that of without catalyst, probably due to saturated octahedron geometry of all Co^{2+} ions for **1** and **2**. It also indicated that coordinately unsaturated Co^{2+} sites in activated **1** played a significant role in heterogeneous catalytic process.

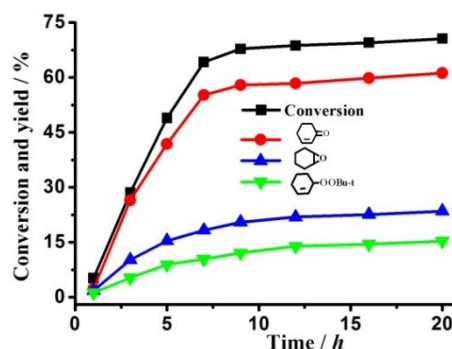
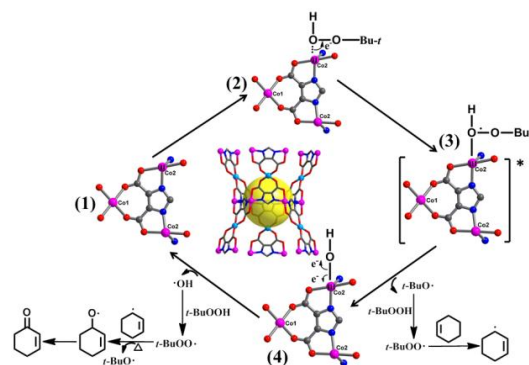


Fig. 6 Conversion and product yields for the allylic oxidation of cyclohexene with ground activated **1** as catalyst at the optimization of reaction condition.

On the basis of our results and previous oxidation of cyclohexene,^{27,28} we propose a possible radical mechanism to elucidate the selectivity (Scheme 1). According to the theory of soft and hard acids and bases, the first step, the Lewis acid Co^{2+} ions of **1** preferentially coordinate by an oxygen atom of *t*-BuOOH. Electrons flow from unsaturated Co^{2+} centers to the peroxy bond of *t*-BuOOH, and form tertbutoxy radicals (*t*-BuO \cdot). The second step: the *t*-BuO \cdot radical quickly abstract a hydrogen atom from another *t*-BuOOH, and create *t*-BuOO \cdot radical, which directly react with cyclohexene to yield 3-cyclohexenyl radical. Then, the *t*-BuOO \cdot radical combines with a 3-cyclohexenyl radical to result in *t*-Bu-cyclohexenyl-1-peroxide, of which the O-O bond thermally decomposes at 70 °C to give main product 2-cyclohexen-1-one. Meanwhile, the cobalt hydroxy species *via* fission of the Co-O bond further recover the initial catalyst **1**, and catalytic cycle starts again.



Scheme 1. A possible oxidation mechanism of cyclohexene with catalyst **1**

To confirm heterogeneous nature of the catalyst, activated **1** was removed from solution by filtration after three hours (approximately 30% conversion). From Fig S10, we can see that activated **1** is a truly heterogeneous catalyst, being no further conversion was observed. The catalyst was easily separated from reaction solution by centrifugation and repeatedly washed which can be regenerated for catalysis. As shown in Fig. 7, there was no significant decrease in catalytic efficiency of activated **1** for allylic oxidation of cyclohexene after five recycles under the optimized conditions. The PXRD pattern of the reused catalyst was similar to that of the fresh catalyst **1** (Fig. S7a), showing the framework of activated **1** was maintained after the catalytic reaction.

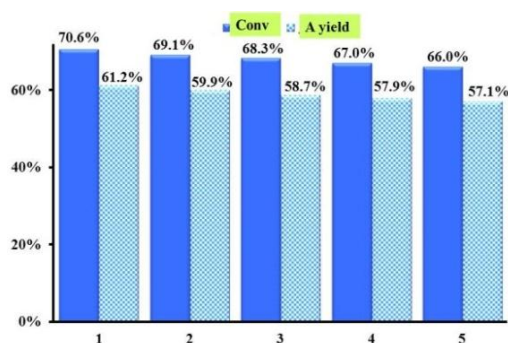


Fig. 7 Recycling tests with activated **1** as catalyst for oxidation reaction of cyclohexene, yield of 2-cyclohexene-1-one.

4. Conclusions

In summary, using 2-position propyl substitutive imidazole-4,5-dicarboxylic acid, two hydrophobic magnetic MOFs with *pcu* net respectively constructed by unique hexagonal Co₆ and zigzag Co₄ clusters, have been successfully synthesized and magnetic characterized. Moreover, activated **1** exhibits high selectivity catalytic activity in the allylic oxidation reaction of cyclohexene to formation of α , β -unsaturated ketone as heterogeneous catalyst. This work may provide an effective strategy to construct hydrophobic MOFs through modify organic ligands and help understand the structure-activity (magnetic and catalytic properties) relations of Co-MOFs materials. In addition, the hydrophobic sites of **1** come from propyl group could be potentially used for separation alkane molecules.

Acknowledgements

Financial support from the 973 Program (2012CB821701), the Ministry of Education of China (Grant IRT1156) and the National Science Fund for Young Scholars (NSFC 20925101 & 21401119) is greatly appreciated. We gratefully acknowledge the assistance in fitting of magnetic properties provided by Jun-Liang Liu.

Notes and references

- (a) M. O'Keeffe and O. M. Yaghi, *Chem. Rev.* 2011, **112** (2), 675; (b) N. Stock and S. Biswas, *Chem. Rev.* 2012, **112** (2), 933.
- (a) J. S. Miller, *Chem. Soc. Rev.* 2011, **40** (6), 3266; (b) P. Dechambenoit and J. R. Long, *Chem. Soc. Rev.* 2011, **40** (6), 3249.
- (a) A. H. Chughtai, N. Ahmad, H. A. Younus, A. Laypkov and F. Verpoort, *Chem. Soc. Rev.* 2015, DOI: 10.1039/C4CS00395K; (b) A. F. Lee, J. A. Bennett, J. C. Manayil and K. Wilson, *Chem. Soc. Rev.* 2014, **43** (22), 7887.
- M. Eddaoudi, D. B. Moler, H. Li, B. Chen, T. M. Reineke, M. O'Keeffe and O. M. Yaghi, *Acc. Chem. Res.* 2001, **34** (4), 319.
- Q.-Q. Wang, V. W. Day and K. Bowman-James, *Chem. Commun.* 2013, **49** (73), 8042.
- J. Fielden, M. Speldrich, C. Besson and P. Kögerler, *Inorg. Chem.* 2012, **51** (5), 2734.
- (a) Y. Han, H. Xu, Y. Liu, H. Li, H. Hou, Y. Fan and S. R. Batten, *Chem-Eur J.* 2012, **18** (44), 13954; (b) S. O. H. Gutschke, D. J. Price, A. K. Powell and P. T. Wood, *Angew. Chem., Int. Ed.* 1999, **38** (8), 1088.
- (a) C. Wang, T. Wang, W. Zhang, H. Lu and G. Li, *Cryst. Growth Des.* 2012, **12** (3), 1091; (b) Y. Zhang, X. Luo, Z. Yang and G. Li, *CrystEngComm* 2012, **14** (21), 7382.
- (a) I. Serrano, M. I. López, Í. Ferrer, A. Poater, T. Parella, X. Fontrodona, M. Solà, A. Llobet, M. Rodríguez and I. Romero, *Inorg. Chem.* 2011, **50** (13), 6044; (b) T. Chantarojsiri, Y. Sun, J. R. Long and C. J. Chang, *Inorg. Chem.* 2015, **54** (12), 5879.
- (a) K. J. Gagnon, C. M. Beavers and A. Clearfield, *J. Am. Chem. Soc.* 2013, **135**, 1252; (b) H.-Y. Ren, R.-X. Yao and X.-M. Zhang, *Inorg. Chem.* 2015, **54**, 6312; (c) N. Zhao, F. Sun, H. He, J. Jia and G. S. Zhu, *Cryst. Growth Des.* 2014, **14**, 1738.
- (a) R.-Q. Fang and X.-M. Zhang, *Inorg. Chem.* 2006, **45** (12), 4801; (b) R.-Q. Fang, X.-H. Zhang and X.-M. Zhang, *Cryst. Growth Des.* 2006, **6** (12), 2637.
- (a) O. Karagiari, M. B. Lalonde, W. Bury, A. A. Sarjeant, O. K. Farha and J. T. Hupp, *J. Am. Chem. Soc.* 2012, **134** (45), 18790; (b) D. F. Sava, V. C. Kravtsov, J. Eckert, J. F. Eubank, F. Nouar and M. Eddaoudi, *J. Am. Chem. Soc.* 2009, **131** (30), 10394; (c) Y.-Y. Zhang, X.-Y. Shen, L.-H. Weng and G.-X. Jin, *J. Am. Chem. Soc.* 2014, **136** (44), 15521.
- (a) R.-R. Zeng, Q.-G. Zhai, S.-N. Li, Y.-C. Jiang and M.-C. Hu, *CrystEngComm* 2011, **13** (15), 4823; (b) F. Zhang, Z. Li, T. Ge, H. Yao, G. Li, H. Lu and Y. Zhu, *Inorg. Chem.* 2010, **49** (8), 3776; (c) J.-H. Deng, D.-C. Zhong, X.-Z. Luo, H.-J. Liu and T.-B. Lu, *Cryst. Growth Des.* 2012, **12** (10), 4861.
- (a) C.-T. He, L. Jiang, Z.-M. Ye, R. Krishna, Z.-S. Zhong, P.-Q. Liao, J. Xu, G. Ouyang, J.-P. Zhang and X.-M. Chen, *J. Am. Chem. Soc.* 2015, **137** (22), 7217; (b) C.-T. He, J.-Y. Tian, S.-Y. Liu, G. Ouyang, J.-P. Zhang and X.-M. Chen, *Chem. Sci.* 2013, **4** (1), 351.
- CrysAlisPro, Agilent Technologies, Version 1.171.37.35 (release 13-08-2014 CrysAlis171 .NET).
- Sheldrick, SHELX-97: Program for X-ray Crystal Structure Solution and Refinement; Göttingen University: Germany, 1997.
- (a) S. Bhattacharya, M. Gnanavel, A. J. Bhattacharyya and S. Natarajan, *Cryst. Growth Des.* 2014, **14** (1), 310; (b) J. P. Zhao, W. C. Song, R. Zhao, Q. Yang, B. W. Hu and X. H. Bu, *Cryst. Growth Des.* 2013, **13**, 2858.
- (a) C. G. Perkins, J. E. Warren, A. Fateeva, K. C. Stylianou, A. McLennan, K. Jelfs, D. Bradshaw and M. J. Rosseinsky, *Micropor. Mesopor. Mater.* 2012, **157**, 24; (b) Z.-Y. Liu, E.-C. Yang, L.-L. Li and X.-J. Zhao, *Dalton Trans.* 2012, **41**, 6827.
- D. Aguila, L. A. Barrios, O. Roubeau, S. J. Teat and G. Aromi, *Chem. Commun.* 2011, **47** (2), 707.
- J.-D. Leng, S.-K. Xing, R. Herchel, J.-L. Liu and M.-L. Tong, *Inorg. Chem.* 2014, **53** (11), 5458.

ARTICLE

Journal Name

- 21 (a) R. X. Yao, Y. L. Qin, F. Ji, Y. F. Zhao and X. M. Zhang, , *Dalton Trans* 2013, **42** (18), 6611; (b) E.-C. Yang, Z.-Y. Liu, T.-Y. Liu, L.-L. Li and X.-J. Zhao, *Dalton Trans.* 2011, **40** (32), 8132.
- 22 R.-X. Yao, X. Cui, J. Wang and X.-M. Zhang, *Chem. Commun.* 2015, **51** (24), 5108.
- 23 P. Díaz-Gallifa, O. Fabelo, J. Pasán, L. Cañadillas-Delgado, J. Rodríguez-Carvajal, F. Lloret, M. Julve and C. Ruiz-Pérez, *Inorg. Chem.* 2014, **53** (11), 5674.
- 24 E. F. Murphy, T. Mallat and A. Baiker, *Catal. Today*, 2000, **57**, 115.
- 25 J. Mao, X. Hu, H. Li, Y. Sun, C. Wang and Z. Chen, *Green Chem.*, 2008, **10**, 827.
- 26 M. Tonigold, Y. Lu, A. Mavrandonakis, A. Puls, R. Staudt, J. Möllmer, J. Sauer and D. Volkmer, *Chem. Eur. J.* 2011, **17**, 8671.
- 27 I. Y. Skobelev, A. B. Sorokin, K. A. Kovalenko, V. P. Fedin and O. A. Kholdeeva, *J. Catal.*, 2013, **298**, 61.
- 28 Y. H. Cao, H. Yu, F. Peng and H. J. Wang, *ACS Catal.* 2014, **4**, 1617.